Chalmers Publication Library

Copyright Notice

(Article begins on next page)

An RF Carrier Bursting System using Partial Quantization Noise Cancellation

Ulf Gustavsson, Thomas Eriksson, Hossein Mashad Nemati, Paul Saad, *Student Member, IEEE,* Peter Singerl, and Christian Fager, *Member, IEEE*

Abstract—This paper introduces a novel method for bandpass cancellation of the quantization noise occurring in high efficiency, envelope pulsed transmitter architectures - or carrier bursting. An equivalent complex baseband model of the proposed system, including the $\Sigma\Delta$-modulator and cancellation signal generation, is developed. Analysis of the baseband model is performed, leading to analytical expressions of the power amplifier drain efficiency, assuming the use of an ideal class B power amplifier. These expressions are further used to study the impact of key system parameters, i.e. the compensation signal variance and clipping probability, on the class B power amplifier drain efficiency and signal-to-noise ratio.

The paper concludes with simulations followed by practical measurements in order to validate the functionality of the method and to evaluate the performance-trend predictions made by the theoretical framework in terms of efficiency and spectral purity.

Index Terms—Carrier Bursting, $\Sigma\Delta$-modulation, Noise-Shaped Coding (NSC), Quantization Noise, Pulsed RF transmitter architectures.

I. INTRODUCTION

MODERN wireless communication systems use advanced high order modulation schemes in order to maximize the spectral efficiency of the system. As a consequence, the peak-to-average power ratio (PAPR) of the transmitted signal increases. Traditional linear amplifiers therefore need to be operated over a backed off, low efficiency region most of the time, in order to fulfill the linearity requirements of the system. Thus, measures to increase the efficiency at backed of power are necessary. Commonly used efficiency enhancement techniques include methods like the Doherty amplifier [1], Chireix outphasing systems [2] or Envelope Tracking (ET) [3]. These methods can, however, be quite bulky and adds to the complexity of the system in terms of additional hardware.

Other promising techniques use 1-bit quantization schemes of different forms. These types of schemes map the amplitude

Fig. 1: (a) A principal sketch on how quantization noise needs to be handled by narrow a band filter at the output in pulsed transmitter architectures. (b) A frequency domain sketch of the signals presented in (a).

and phase information of the signal on to certain characteristics of an input signal pulse-train, such as pulse-width, -position or -density (PWM, PPM, PDM), [4]. By applying this type of modulation, the power amplifier only operates in its two most efficient regions - deep saturation or completely off. The methods are usually applied by either directly encoding the modulated RF signal [5], or by encoding the baseband signal before converting to RF [6]. The latter method, which we will focus on in this paper, is commonly referred to as *carrier bursting* due to the fact that the PA is effectively driven by short bursts of phase-modulated RF-carrier. A major drawback with all 1-bit modulation schemes is, however, the large amount of distortion inflicted by the quantization process.

In order to recover the modulated signal before transmission, a filter for signal reconstruction is required as illustrated in Fig. 1a. To keep the pulse-rate low and the intrinsic switch-losses to a minimum, narrowband filters are needed for reconstruction, as illustrated in Fig. 1b. Narrowband filters at

microwave frequencies tend to suffer from large insertion loss [7], which in turn will have a negative impact on the power efficiency.

Several promising techniques have been proposed over the years to remedy the need for narrowband filters. One suggested method uses a feed forward technique [8], a technique commonly used for cancellation of amplifier non-linearities. However, this technique has significant drawbacks due to increased size, cost and complexity in terms of the additional hardware needed for the error-amplifier and time-delay synchronization.

A different approach is to use so called *digitally segmented amplifiers* [9], where n parallel amplifiers are working in a 2^n-weighted formation. In this scheme, each amplifier is weighted according to its binary position in the ladder. This high power, multi-bit digital-to-analogue converter (DAC) approach, in combination with certain shaping of the pulses, provides a good suppression of the residual quantization distortion. But, as in the previous case, this comes at the cost of a large increase of complexity in terms of the n amplifiers needed.

A more common method for suppressing the quantization distortion, which is particularly used in oversampled PDM-modulators, is a method referred to as Noise-Shaped Coding (NSC) [10] or *Noise-shaping*. Here, the encoded signal is mapped on to the characteristics of the pulse-train in a manner for which a majority of the quantization distortion is placed in the stop-band regions of the reconstruction filter. The most common method of implementing NSC is the so called $\Sigma\Delta$-modulator [11], where the NSC-properties are determined by the loop-filters of the structure. NSC is known to improve the error performance of the reconstructed signal for sufficiently large oversampling ratio, which leaves the switch losses an issue remaining to be solved.

This paper presents a simplified pre-compensation based technique, introducing a trade-off where limited amplitude variations are superimposed on the input signal pulses in order to cancel out selected parts of the quantization distortion spectrum, see Fig. 2a. This enables the use of a relatively wideband reconstruction filter, thus enabling high efficiency operation. Throughout this paper, the method is derived for, and demonstrated on, a carrier bursting system [6]. However, the method can with little effort be used in other types of pulsed transmitter architectures.

This method was first introduced in [12], but is presented in more detail here. The trade-off between cancellation signal bandwidth (BW_c), switching frequency, and efficiency is investigated theoretically and verified with experimental results using an existing high efficiency 3.5 GHz GaN class F^{-1} power amplifier [13]. Yet another trade-off introduced here, is that of limiting the range of the amplitude variations by means of clipping, which is known to cause spectral regrowth. Thus, a model-based approach to predict the level of clipping distortion is developed and evaluated.

The paper is organized as follows. In section II, a detailed description of the suggested method is given, followed by a short mathematical analysis of the compensation mechanism. An analytical drain-efficiency model is derived for the case of an ideal class B amplifier in III. Section IV demonstrates the concept by simulations and measurements. A generalization
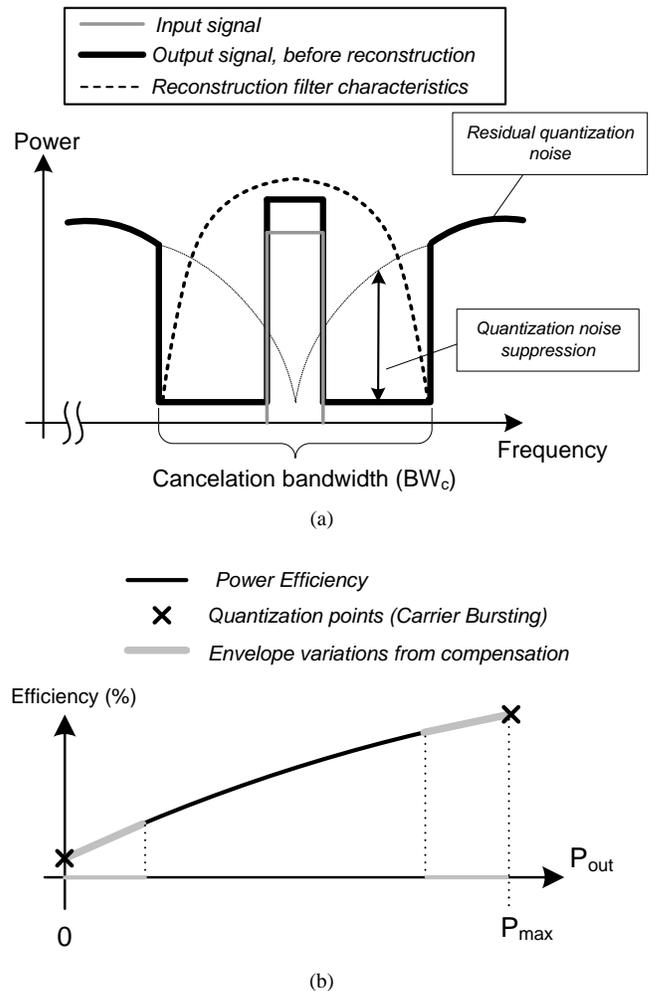
Fig. 2: (a) A view of the quantization-noise free region due to the proposed cancellation method. (b) Illustration of input signal regions and power efficiency vs output power.

of the theoretical framework toward a larger class of pulsed transmitter architectures is described and exemplified in section V.

II. SYSTEM DESCRIPTION

In order to achieve the quantization noise suppression as illustrated in Fig. 2a, a method of calculating and applying a cancellation component is needed. The method proposed in [12] and described in detail here is based on allowing a band- and variance-limited component, derived based on knowledge of the quantization error, to be superimposed on to the pulse-train. Thus, as illustrated in Fig. 2b, the amplifier is operated over regions of output power which are still very efficient, instead of exclusively operating at deep saturation and in cut-off, as in regular carrier bursting. By proper design of the cancellation signal, a spectrum clear of quantization noise over a certain bandwidth around the carrier can be created.

As a result of the suggested cancellation, an increase of fractional bandwidth of the necessary reconstruction filter can be facilitated for any given pulse-rate. This comes at the cost of a slight increase of dissipated power due to the
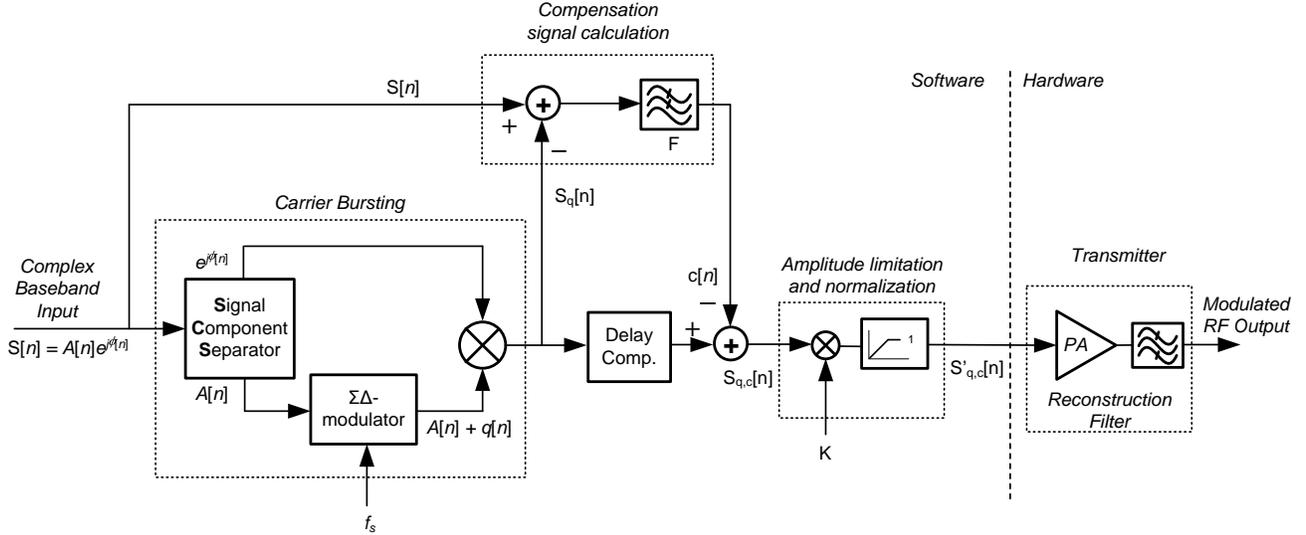
Fig. 3: Complex baseband model illustrating the components of the proposed quantization noise cancellation scheme, applied with a carrier bursting transmitter.

suggested amplitude variations, while potentially reducing the insertion loss of the reconstruction filter. Thus, through the proposed method, the designer is given an additional degree of freedom in trading off reconstruction filter insertion loss and the intrinsic dissipated losses, while keeping the pulse-rate at a minimum to avoid unnecessary switching losses.

The suggested method of cancellation is here shown when implemented with a carrier bursting system, see Fig. 3. The figure includes a linear phase FIR-filter, $F(\omega)$, which determines the compensation bandwidth, denoted BW_c in Fig. 2a. If the passband of $F(\omega)$ increases, then BW_c increases accordingly which, as will be shown, results in larger amplitude variance of the cancellation signal, reducing the PA power efficiency.

A. The carrier bursting part

We will now move on to provide a mathematical description of the complex equivalent baseband model as shown in Fig. 3. The complex valued communication signal, $S[n]$, applied to the system can be expressed in polar form as

$$S[n] = A[n]e^{i\varphi[n]} \tag{1}$$

It should be noted here that $S[n]$ needs to be sparse in frequency, i.e. that a sample-rate for which the $\Sigma\Delta$-modulator performs appropriately is used. This sample-rate is denoted by f_s in Fig. 3. It is further assumed that $S[n]$ is wide-sense stationary (WSS), which in turn implies that all signals derived from $S[n]$ are WSS. Bennett's theorem, [14, p. 48, eq.(2.3)], implies that this holds for (ideal) $\Sigma\Delta$-modulation.

Now, $S[n]$ is separated in to an amplitude component, $A[n]$, and a phase component, $e^{i\varphi[n]}$ using the signal component separator. $A[n]$ is then quantized separately using a 1-bit $\Sigma\Delta$-modulator. The quantization process in turn adds a quantization error term, $q[n]$, which results in a binary amplitude component

$$A_q[n] = A[n] + q[n] \in \{0, 1\}. \tag{2}$$

It should be noted here that the spectrum of the $q[n]$ component is determined by the NSC-properties of the $\Sigma\Delta$-modulator, thus also determining the Power Spectral Density (PSD) of the quantized amplitude signal $A_q[n]$. The binary amplitude-component is now recombined with the phase-component, which gives us the new signal

$$S_q[n] = A_q[n]e^{i\varphi[n]} = (A[n] + q[n])\,e^{i\varphi[n]}$$

$$= \underbrace{S[n]}_{\text{Original Signal}} + \underbrace{q[n]e^{i\varphi[n]}}_{\text{Quantization error}} \tag{3}$$

which, as described above, has a binary envelope and includes a now phase-modulated quantization error term.

B. The compensation signal

In order to facilitate the use of wideband reconstruction filters, we now seek to cancel out the error term $q[n]e^{i\varphi[n]}$ over a frequency band BW_c, as illustrated in Fig. 2a. For this purpose, the linear phase low pass filter $F(\omega)$ is utilized. Passing $q[n]e^{i\varphi[n]}$ through F, as shown in Fig. 3, creates the desired cancellation component $c[n]$, which is subtracted from the amplitude-quantized signal $S_q[n]$.

For a given cancellation filter $F(\omega)$, with impulse response $\{f[k]\}_{k=0}^{M}$ of length M, which can be infinite, we can now calculate the cancellation component $c[n]$ as

$$c[n] = \sum_{k=-\infty}^{+\infty} f[k]q[n-k]e^{i\varphi[n-k]} \tag{4}$$

Without loss of generality, we can for the purpose of our analysis assume that the filter $F(\omega)$ has no delay and normalized passband gain. In practice however, the delay caused by the linear phase filter $F(\omega)$ needs to be compensated for by delaying the quantized signal $S_q[n]$ before applying the compensation signal, $c[n]$, as shown in Fig. 3. The linear phase requirement of $F(\omega)$ could also be relaxed if an equalizer

is introduced instead of, or in combination with, the delay compensation. This results in the following expression.

$$\begin{aligned} S_{q,c}[n] &= S_q[n] - c[n] \\ &= A[n]e^{i\varphi[n]} + q[n]e^{i\varphi[n]} - c[n] \end{aligned} \quad (5)$$

The new signal, which now also contains the compensation signal, can in frequency domain be written in as the sum of the original signal and the residual highpass quantization distortion term,

$$\Phi_{S_{q,c}}(\omega) = \Phi_S(\omega) + (1 - |F(\omega)|^2)\Phi_q(\omega) \quad (6)$$

since

$$\Phi_c(\omega) = |F(\omega)|^2 \Phi_q(\omega) \quad (7)$$

where the power spectrum terms of the signal, $\Phi_S(\omega)$, the quantization error, $\Phi_q(\omega)$, and the compensation signal, $\Phi_c(\omega)$, are calculated by Fourier-transforming the autocorrelation functions of $S[n]$, $q[n]e^{i\varphi[n]}$ and $c[n]$ respectively. Thus, the cutoff frequency of $F(\omega)$ determines BW_c.

Interesting observations can now be made by studying (3)-(6) in two extreme cases for the cancellation filter, $F(\omega)$. It is easily shown that for the case where the bandwidth of $c[n]$ approaches $f_s/2$, i.e. when $F(\omega)$ approaches an all-pass filter with the impulse response $\delta[n]$, we will have that

$$\begin{aligned} c[n] &= \sum_{k=-\infty}^{+\infty} f[k]q[n-k]e^{i\varphi[n-k]} \\ &\rightarrow \sum_{k=-\infty}^{+\infty} \delta[n]q[n-k]e^{i\varphi[n-k]} \\ &= q[n]e^{i\varphi[n]} \end{aligned} \quad (8)$$

Thus, applying (8) to (6), we see that

$$BW_c \rightarrow \frac{f_s}{2} \Rightarrow S_{q,c}[n] \rightarrow S[n] \quad (9)$$

In other words, these results show that when an all pass filter (or a constant) is used for $F(\omega)$, the modulator output signal, S_{qc}, is identical to the input signal. This corresponds to a regular linear mode of operation rather than a carrier bursting operation.. Turning the cutoff frequency of $F(\omega)$ in the other direction, e.g. for BW_c approaching zero, we will have that

$$c[n] = \sum_{k=-\infty}^{+\infty} f[n-k]q[n]e^{i\varphi[n]} \rightarrow 0 \quad \forall n \quad (10)$$

which is to say that the system approaches the regular carrier bursting system with a binary output signal. These two extreme cases demonstrate the merging of a digital and a analogue (or discrete binary and continuous) domain in the suggested system, in which the degree of digital/analogue mixture is set on a sliding scale by the filter $F(\omega)$.

III. SYSTEM ANALYSIS

Using the system description above, we will now proceed by developing a theoretical framework for the power amplifier drain efficiency performance. This model will be used to illustrate the trade-offs between efficiency and key parameters

of the proposed cancellation scheme. The model will be derived assuming an ideal class B amplifier, described in [15], and the probability density function (PDF) of the composite signal envelope. It should be noted that the analysis is, for simplicity, idealized and performed without regarding the interaction between the PA and the reconstruction filter.

A. An ideal class B-based efficiency framework

The average drain efficiency, η, for a general modulated signal may be expressed as the average output power, P_{out}, divided by the average consumed DC-power, P_{DC},

$$\eta = \frac{P_{\text{out}}}{P_{\text{DC}}} \quad (11)$$

We will here consider a normalized and perfectly linear power amplifier model in which $|S_{q,c}[n]| \in [0,1]$ is the voltage at the power amplifier output, from which it becomes straight forward to express the RF output power in (11) as

$$P_{\text{out}} = \mathbb{E}\left[|S_{q,c}[n]|^2\right]. \quad (12)$$

Assuming an ideal, normalized class B amplifier, it then follows that the DC-power can be described as [15]

$$P_{\text{DC}} = \frac{4}{\pi}\sqrt{P_{\text{out}}} = \frac{4}{\pi}\mathbb{E}\left[|S_{q,c}[n]|\right] \quad (13)$$

Using (11), (13) and (12) for an ideal class B amplifier with a normalized load [15], the drain efficiency is now easily calculated as

$$\eta_B = \frac{\pi}{4} \cdot \frac{\mathbb{E}\left[|S_{q,c}[n]|^2\right]}{\mathbb{E}\left[|S_{q,c}[n]|\right]} \quad (14)$$

Following the assumption of an ideal class B PA, the amplifier is assumed to be linear and $|S_{q,c}[n]|$ represents therefore the output amplitude preceding the reconstruction filter. Thus, in order to derive a closed form expression for the drain efficiency we need to obtain knowledge of the PDF of the envelope of the composite signal, $|S_{q,c}[n]|$.

First, the probability of each quantizer-state occurring is denoted as

$$\begin{aligned} \lambda_0 &= \Pr(A_q = 0) \\ \lambda_1 &= \Pr(A_q = 1) \end{aligned} \quad (15)$$

where $\lambda_0 + \lambda_1 = 1$. Now, each outcome of $S_{q,c}[n]$, conditioned on the binary $\Sigma\Delta$-modulator state, $A_q[n] \in \{0,1\}$, are assumed to be a complex Gaussian distributions,

$$S_{q,c} \sim \mathcal{CN}\left(A_q, \sigma_c^2\right). \quad (16)$$

From the above, it follows by [16, p.565-567] that the magnitude, $|S_{q,c}[n]|$, in both cases, will have a Rician PDF [17] - $r_{|S_{q,c}|}(s|0, \sigma_c)$ and $r_{|S_{q,c}|}(s|1, \sigma_c)$. Finally, as a result of the law of total probability [18], we can write the PDF of $|S_{q,c}[n]|$ as a mixture distribution

$$p_{|S_{q,c}|}(s|\boldsymbol{\nu}, \boldsymbol{\sigma}) = \lambda_0 r_{|S_{q,c}|}(s|0, \sigma_c) + \lambda_1 r_{|S_{q,c}|}(s|1, \sigma_c), \quad (17)$$

where $\boldsymbol{\sigma} = \{\sigma_c^2, \sigma_c^2\}$, σ_c^2 is the variance of the cancellation signal and $\boldsymbol{\nu} = \{0, 1\}$. Two major simplifications now follows, under the assumption that σ_c^2 is small. First, we note that $r_{|S_{q,c}|}(s|0, \sigma_c)$ collapses to a Rayleigh-distribution. Similarly,
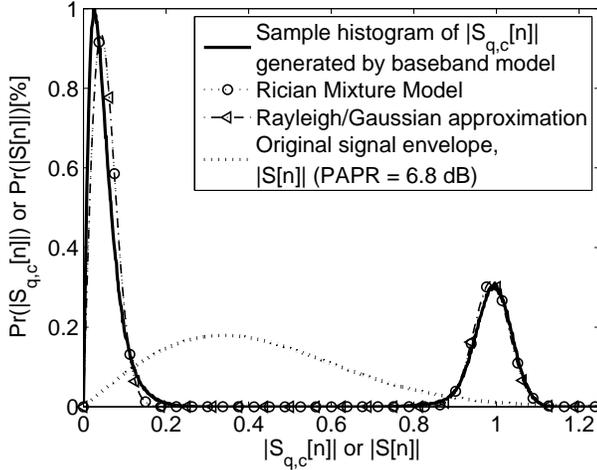
Fig. 4: Sample histogram of a simulated $|S_{q,c}[n]|$ and a fitted Rician mixture model for $BW_c = f_s/4$.

since $\sigma_c^2 << 1$, we can further simplify the expression by approximating $r_{|S_{q,c}|}(s|1,\sigma_c)$ with a Gaussian distribution - $\mathcal{N}(1,\sigma_c^2)$, [19].

One example of the Rician mixture model and the Gaussian/Rayleigh approximation is shown in Fig. 4. These results have been obtained with a 1 carrier W-CDMA input signal using the generalized $\Sigma\Delta$-modulator structure presented in [20].

Finally, assuming ideal low-pass $\Sigma\Delta$-modulation, i.e that for a fixed BW_c

$$\lim_{f_s \to +\infty} \sigma_c^2 \to 0, \quad (18)$$

we can make the observation that the peak-to-average power ratio (PAPR) of $|S[n]|$ is connected to λ_1 as

$$\lambda_1 = 10^{-\text{PAPR}/10}, \quad (19)$$

since $S_q[n]$ is, as a result of being derived from $S[n]$, WSS.

B. Clipping and signal scaling

Since the ideal normalized class B amplifier model is defined only over the amplitude domain $[0, 1]$, it will be incompatible with the mixture model $p_{|S_{q,c}|}$, which is built up using PDFs that have infinite support. Therefore, the probability of truncating or clipping the signal when $|S_{q,c}[n]| > 1$ needs to be considered, since $|S_{q,c}[n]| = 1$ would correspond to the maximum feasible output amplitude. Further on, although said clipping of the signal results in undesirable distortion, clipping can be used to some extent for improving the power amplifier efficiency. Thus, for the ideal class B efficiency model, we need expressions for calculating the normalization constant, K, for which we achieve an arbitrary desired clipping probability $\mathcal{K} = \Pr(K|S_{q,c}[n]| > 1)$ after the limiter, as shown in Fig. 3.

Before proceeding with the development of these expressions, some approximations can be made in order to simplify the forthcoming analysis under the assumption that σ_c^2 is, numerically, very small due to the use of optimized NSC.

Starting with $r_{|S_{q,c}|}(s|0,\sigma_c)$, we know that the Rayleigh distribution is supported over the interval $[0, +\infty)$. However, we can conclude that a dominating part of the distribution is located within $[0, 1]$. Thus, the remaining outliers above $|S_{q,c}[n]| = 1$ that are contributed by $r_{|S_{q,c}|}(s|0,\sigma_c)$ are numerically insignificant and can be safely discarded from the model.

And since the envelope $|S_{q,c}[n]|$ only takes positive values, and the Gaussian distribution is supported on $(-\infty, +\infty)$, we need to eliminate any contributions from the Gaussian approximation of $r_{|S_{q,c}|}(s|1,\sigma_c)$ for negative arguments, since these will not occur in reality. However, since $r_{|S_{q,c}|}(s|1,\sigma_c)$ is centered around 1, before clipping and normalization, and σ_c^2 is assumed to be very small, we can further simplify our calculations by truncating the left tail of $r_{|S_{q,c}|}(s|1,\sigma_c)$, since these contributions will be numerically very close to zero. The conditions stated above justifies two approximations, which can be made in order to simplify the analytical class B drain efficiency model. These are

$$\int_0^1 s^n r_{|S_{q,c}|}(s|0,\sigma_c)\, ds \approx \int_0^{+\infty} s^n r_{|S_{q,c}|}(s|0,\sigma_c)\, ds \quad (20)$$

and

$$\int_0^1 s^n r_{|S_{q,c}|}(s|1,\sigma_c)\, ds \approx \int_{-\infty}^1 s^n r_{|S_{q,c}|}(s|1,\sigma_c)\, ds, \quad (21)$$

for both $n = 1$ and $n = 2$.

The same principle can not be applied for the case of $r_{|S_{q,c}|}(s|1,\sigma_c)$ for $|S_{q,c}[n]| > 1$ due to its location, even for very small σ_c^2. For this purpose, and in the interest of keeping the power amplifier at high efficiency operation, a combined normalization and amplitude limiter is introduced as shown in Fig. 3. This process can be implemented for any desired clipping probability by following the next few steps.

Assuming, as stated above, that $r_{|S_{q,c}|}(s|1,\sigma_c)$ is the dominant mixture component for $|S_{q,c}[n]|$ close to 1, we can in a simplified manner define the expression for the desired clipping-probability $\mathcal{K}$ as

$$\mathcal{K} = \lambda_1 \int_{\frac{1}{K}}^{+\infty} r_{|S_{q,c}|}(s|1,\sigma_c)\, ds \quad (22)$$

where $\frac{1}{K}$ is the value of $|S_{q,c}[n]|$ at which the desired clipping probability occurs. Solving for K then gives us the normalizing constant, which is applied to $|S_{q,c}[n]|$. K is calculated as

$$K = \frac{1}{1 + \sqrt{2}\sigma_c \text{erfc}^{-1}\left[\frac{2\mathcal{K}}{\lambda_1}\right]}. \quad (23)$$

After applying the normalization, the limiter can simply clip all samples with magnitude larger than 1 in order to achieve $\mathcal{K}\%$ of clipped samples. This results in the clipped signal, $S'_{q,c}[n]$, described as

$$S'_{q,c}[n] = \begin{cases} K\dfrac{S_{q,c}[n]}{|S_{q,c}[n]|} & \text{if } K|S_{q,c}[n]| > 1 \\[2mm] KS_{q,c}[n] & \text{else.} \end{cases} \quad (24)$$

Fig. 5 shows one example of the signal envelope PDF before ($|S_{q,c}[n]|$) and after ($|S'_{q,c}[n]|$) clipping with $\mathcal{K} = 1\%$.
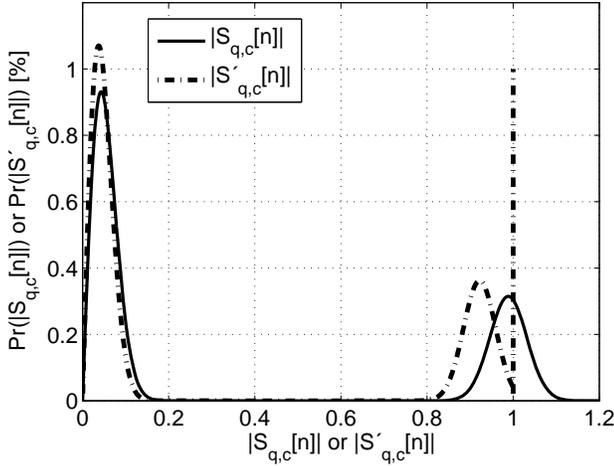
Fig. 5: The Rician mixture model of $|S_{q,c}[n]|$ and its clipped version, $|S'_{q,c}[n]|$, using a clipping probability $\mathcal{K} = 1\%$ and $BW_c = f_s/4$.

The clipped signal envelope, $|S'_{q,c}|$, now has a slightly different PDF, described by the mixture

$$
\begin{aligned}
p_{|S'_{q,c}|}(s|\boldsymbol{\nu},\boldsymbol{\sigma}) &= \lambda_0 \mathbf{I}_{[0,1]}(s) r_{|S_{q,c}|}(s|0,\sigma_{kc}) \\
&+ \lambda_1 \mathbf{I}_{[0,1]}(s) r_{|S_{q,c}|}(s|K,\sigma_{kc}) \\
&+ \mathcal{K}\delta(s-1)
\end{aligned}
\tag{25}
$$

where $\mathbf{I}_{[0,1]}(s)$ is the indicator function

$$
\mathbf{I}_{[0,1]}(s) = \begin{cases} 1 & \text{if } s \in [0,1] \\ 0 & \text{else.} \end{cases}
\tag{26}
$$

and $\sigma_{kc}^2 = K^2 \sigma_c^2$. Given that $r_{|S_{q,c}|}(s|0,\sigma_{kc})$ and $r_{|S_{q,c}|}(s|1,\sigma_{kc})$ are Rician distributions, $p_{|S'_{q,c}|}(s|\boldsymbol{\nu},\boldsymbol{\sigma})$ hold the properties of a PDF with support $[0,1]$.

C. Connecting Noise-Shaped Coding and Efficiency

In order to further illustrate the impact and importance of NSC, we need to analytically examine the compensation signal variance σ_c^2. From [21, p. 828, eq. 12.1.19], we see that σ_c^2 can be written as

$$
\sigma_c^2 = \mathbb{E}\left[|c[n]|^2\right] = \phi_c(0),
\tag{27}
$$

where ϕ_c denotes autocorrelation function of $c[n]$. This can then be calculated using the Wiener-Khinchin theorem and the PSD of $c[n]$, $\Phi_c(\omega)$, as presented in (7)

$$
\begin{aligned}
\phi_c(0) &= \frac{1}{2\pi} \int_{-\pi}^{+\pi} \Phi_c(\omega) d\omega \\
&= \frac{1}{2\pi} \int_{-\pi}^{+\pi} |F(\omega)|^2 \Phi_q(\omega) d\omega.
\end{aligned}
\tag{28}
$$

Apart from the spectrum of the phase-component, $e^{i\varphi[n]}$ in (5), we can assume that the spectrum of the output quantization noise, $\Phi_q(\omega)$, is determined by the Noise Transfer Function (NTF) of the $\Sigma\Delta$-modulator. This is written as

$$
\Phi_q(\omega) = \sigma_q^2 |NTF(\omega)|^2
\tag{29}
$$

where $\sigma_q^2 = \Delta^2/12$ [22], in which $\Delta = 1$ for the quantizer defined in (2). For further simplifications, we approximate $|F(\omega)|^2$ by a brickwall-filter

$$
|F(\omega)|^2 = \begin{cases} 1 & \text{if } |\omega| \leq \pi BW_c \\ 0 & \text{else,} \end{cases}
\tag{30}
$$

which lets us rid the equation (28) of the filter-term $|F(\omega)|^2$ by simply adjusting the integration interval from $[-\pi, +\pi]$ to $[-\pi BW_c, +\pi BW_c]$. And by using the symmetry of $|\text{NTF}(\omega)|^2$ around $\omega = 0$, we get a simplified expression for calculating σ_c^2 as

$$
\begin{aligned}
\sigma_c^2 &= \frac{1}{24\pi} \int_{-\pi}^{\pi} |F(\omega)| \cdot |\text{NTF}(\omega)|^2 d\omega \\
&= \frac{1}{24\pi} \int_{-\pi BW_c}^{\pi BW_c} |\text{NTF}(\omega)|^2 d\omega \\
&= \frac{1}{12\pi} \int_{0}^{\pi BW_c} |\text{NTF}(\omega)|^2 d\omega
\end{aligned}
\tag{31}
$$

One very important implication of (31) is that the amplifier operation regions, which are shown here to be dependent on σ_c^2, can be reduced for a given pulse-rate by deploying an optimized NSC scheme in order to selectively reduce the quantization noise energy within the frequency-band of interest, BW_c. This, in turn, results in improved power efficiency due to reduction of the dissipated power.

In order to exemplify the analysis made above, we can study a general N^{th} order integrator-based low-pass $\Sigma\Delta$-modulator with the NTF described by

$$
\text{NTF}(\omega) = (1 - e^{j\omega})^N
\tag{32}
$$

for integer $N \geq 1$. Inserting (32) into (31) yields the expression

$$
\sigma_c^2 = \frac{1}{12\pi} \int_{0}^{\pi BW_c} \left[2\sin\left(\frac{\omega}{2}\right)\right]^{2N} d\omega.
\tag{33}
$$

Using the fundamental theorem of analysis, solving the above integral yields the result

$$
\begin{aligned}
\sigma_c^2 &= \frac{2^{2N+1}}{12\pi} \left[{}_2F_1\left(\frac{1}{2}, \frac{1}{2} - N, \frac{3}{2} \middle| 1\right) \right. \tag{34} \\
&- \left. \cos\left(\frac{\pi BW_c}{2}\right) {}_2F_1\left(\frac{1}{2}, \frac{1}{2} - N, \frac{3}{2} \middle| \cos^2\left(\frac{\pi BW_c}{2}\right)\right) \right]
\end{aligned}
$$

where ${}_2F_1$ is the Gaussian hypergeometric function. Examples of σ_c^2 from both signal record calculations and estimations using (35) for $N = 1$ and 2, as a function of BW_c/f_s, is shown in Fig. 6. It is plotted normalized to the quantization noise variance, σ_q^2, in order to illustrate that for $BW_c \to f_s/2$, $\sigma_c^2 \to \sigma_q^2$.

For the generalized $\Sigma\Delta$-modulator with IIR loop-filters $H(e^{j\omega})$ and $G(e^{j\omega})$, [20, eq. (35)] provides the analytical expression for the NTF. For a short notation, we define

$$
P(e^{j\omega}) = H(e^{j\omega})G(e^{j\omega}),
\tag{35}
$$

which provides the expression for calculating σ_c^2 as

$$
\sigma_c^2 = \frac{1}{12\pi} \int_{0}^{+\pi BW_c} \frac{d\omega}{|P(e^{j\omega})|^2 + 2\text{Re}(P(e^{j\omega})) + 1}.
\tag{36}
$$
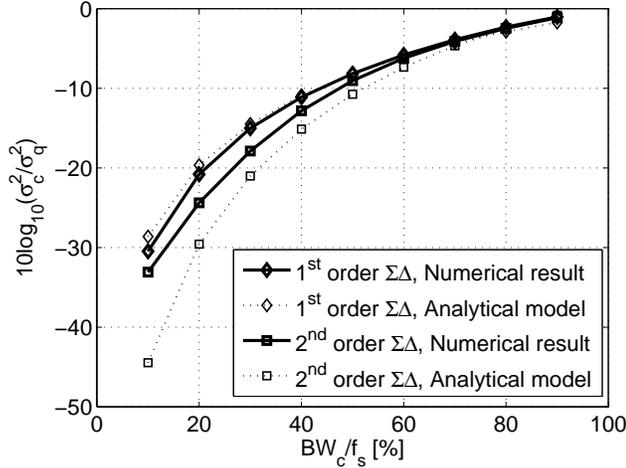
Fig. 6: Both numerically determined and analytically modeled values for σ_c^2 given $N = 1, 2$ order $\Sigma\Delta$-modulators.

Fig. 7: Calculated class B drain efficiency as a function of fractional compensation bandwidth, BW_c/f_s, and clipping probability, $\mathcal{K}$, using the expression stated in (37). Here with $PAPR = 6.8$ dB, i.e. $\lambda_1 \approx 0.2$.

And since the denominator is a real-valued rational function, the integration becomes a straight forward procedure.

D. Model-based efficiency prediction

As we now have developed expressions for the envelope PDF, it is straight forward to form the expression for the average efficiency using the ideal class B amplifier model. By assembling the results from III-A with III-B and (14), a final closed expression for the ideal class B drain efficiency estimate can be formed as presented in (37), where $Q()$ is the Q-function [23]. Since the clipped samples take the magnitude $|S'_{q,c}[n]| = 1$ after normalization, they will correspond to peak efficiency of $\pi/4$ according to the ideal class B assumptions.

Using this model, we can calculate η_B over a range of σ_{kc}^2, calculated as described in section III-C, and $\mathcal{K}$, which produces the surface shown in Fig. 7. The figure shows that there is a strong connection between the NSC-performance, i.e. σ_c^2, and the power amplifier efficiency. It also shows that the effects of clipping on η_B is decreasingly significant as $\sigma_c^2 \to 0$.

From (37) it also becomes quite clear that for the special case presented in (9) where $BW_c \to 0$, we get that $\sigma_c^2 \to 0$, from which it follows that we from (23) get $K \to 1$. These results will then yield the estimate $\eta_B = \frac{\pi}{4}$, which corresponds to the peak efficiency of an ideal class B amplifier, as expected according to the idealized assumption.

E. Model-based clipping distortion prediction

It is important to note that when increasing the probability of clipping the signal, distortion and spectral regrowth will occur. Thus, predicting the in-band Signal-to-Noise Ratio (SNR) degradation by modeling of the clipping distortion becomes crucial. This is needed in order to determine a suitable value for $\mathcal{K}$ which provides the best possible efficiency-distortion trade-off as possible, while operating within the spectral requirements of the system.

Assuming that the clipping distortion has a white spectrum, we can use a very simple approximation in order to estimate
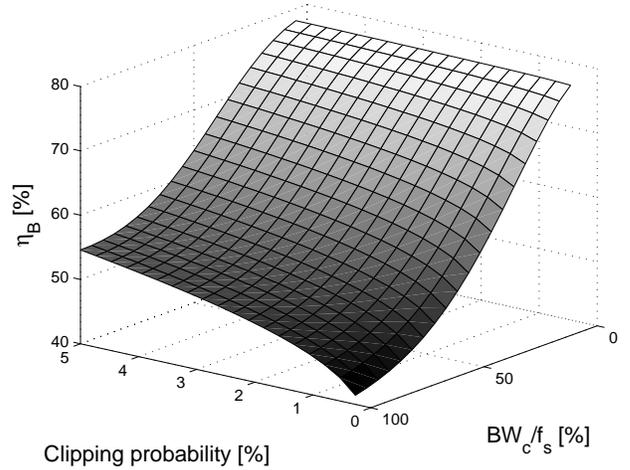
the resulting SNR as shown here. The spectrum of the clipped signal will be approximated using a linear additive white Gaussian noise (AWGN) model

$$S'_{q,c}[n] = KS_{q,c}[n] + w[n] \tag{38}$$

where $w \sim \mathcal{CN}\left(0, \sigma_w^2\right)$ with spectrum $\Phi_w(\omega) = \sigma_w^2$. In order to determine σ_w^2, we need to know the power contained in the clipped samples. The variance of a truncated Gaussian signal is derived in [24] and yields

$$\sigma_w^2 = \lambda_1 \sigma_{kc}^2 \left(1 - \frac{g(\alpha)}{1 - G(\alpha)} \left[\frac{g(\alpha)}{1 - G(\alpha)} - \alpha \right] \right) \tag{39}$$

where $g(\alpha)$ is the PDF and $G(\alpha)$ the CDF of the standard normal distribution, $\mathcal{N}(0, 1)$, with parameter $\alpha = \frac{1-K}{\sigma_{kc}}$. The in-band SNR estimate, SNR_{est}, is then calculated as

$$\text{SNR}_{\text{est}} = 10 \log_{10} \left(\frac{\displaystyle\int_{BW_c} \Phi_S(\omega)\, d\omega}{\displaystyle\int_{BW_c} \Phi_w(\omega)\, d\omega} \right) \tag{40}$$

where $\Phi_S(\omega)$ is the spectrum of $S[n]$. Here, the numerator can be quickly recognized as the variance of $S[n]$, σ_s^2, and since only the parts of $\Phi_w(\omega)$ contained within BW_c are of interest, the denominator reduces to

$$\int_{BW_c} \Phi_w(\omega)\, d\omega = \frac{BW_c}{f_s} \sigma_w^2 \tag{41}$$

due to the whiteness of w. Finally, assembling the above yields the SNR estimate as

$$\text{SNR}_{\text{est}} = 10 \log_{10} \frac{f_s}{BW_c} \frac{\sigma_S^2}{\sigma_w^2}. \tag{42}$$

The validity of this estimate is examined by simulations, comparing the estimate with actual clipped signal records, in the next chapter.

$$
\begin{aligned}
\eta_B &= \frac{\pi}{4} \cdot \frac{\displaystyle\int_0^1 s^2 p_{|S'_{q,c}|}(s|\boldsymbol{\nu},\boldsymbol{\sigma})\,ds}{\displaystyle\int_0^1 s p_{|S'_{q,c}|}(s|\boldsymbol{\nu},\boldsymbol{\sigma})\,ds} = \frac{\pi}{4} \cdot \frac{\lambda_0 \displaystyle\int_0^1 s^2 r_{|S'_{q,c}|}(s|0,\sigma_{kc})\,ds + \lambda_1 \displaystyle\int_0^1 s^2 r_{|S'_{q,c}|}(s|K,\sigma_{kc})\,ds + \mathcal{K}}{\lambda_0 \displaystyle\int_0^1 s r_{|S'_{q,c}|}(s|0,\sigma_{kc})\,ds + \lambda_1 \displaystyle\int_0^1 s r_{|S'_{q,c}|}(s|K,\sigma_{kc})\,ds + \mathcal{K}} \\[2ex]
&\approx \frac{\pi}{4} \cdot \frac{\lambda_0 \displaystyle\int_0^{+\infty} s^2 r_{|S'_{q,c}|}(s|0,\sigma_{kc})\,ds + \lambda_1 \displaystyle\int_{-\infty}^1 s^2 r_{|S'_{q,c}|}(s|K,\sigma_{kc})\,ds + \mathcal{K}}{\lambda_0 \displaystyle\int_0^{+\infty} s r_{|S'_{q,c}|}(s|0,\sigma_{kc})\,ds + \lambda_1 \displaystyle\int_{-\infty}^1 s r_{|S'_{q,c}|}(s|K,\sigma_{kc})\,ds + \mathcal{K}} \\[2ex]
&= \frac{\pi}{4} \cdot \frac{2\lambda_0 \sigma_{kc}^3 + \lambda_1 \left[(K^2+\sigma_{kc}^2) Q\left(\dfrac{K-1}{\sigma_{kc}}\right) - \dfrac{\sigma_{kc}(1+K)}{\sqrt{2\pi}} e^{\frac{-(K-1)^2}{2\sigma_{kc}^2}} \right] + \mathcal{K}}{\lambda_0 \sigma_{kc}^2 \dfrac{\sqrt{\pi}}{\sqrt{2}} + \lambda_1 \left[K Q\left(\dfrac{K-1}{\sigma_{kc}}\right) - \dfrac{\sigma_{kc}}{\sqrt{2\pi}} e^{\frac{-(K-1)^2}{2\sigma_{kc}^2}} \right] + \mathcal{K}}
\end{aligned}
\tag{37}
$$
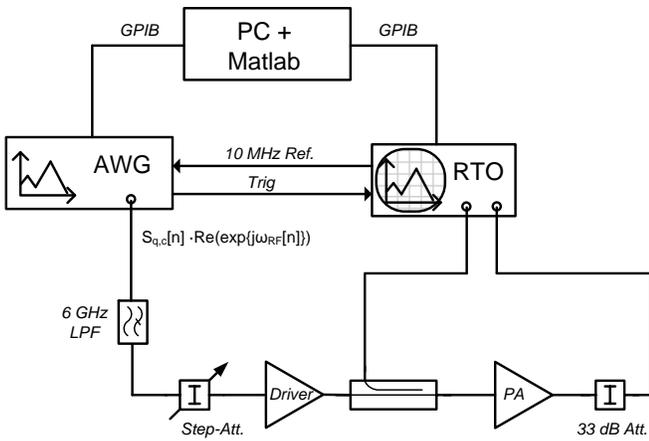
Fig. 8: A block schematic of the measurement setup.

IV. EXPERIMENTAL RESULTS

A. Prerequisites

In order to experimentally validate the proposed system, the equivalent complex baseband model was implemented in MATLAB. Measurements were then performed using the class F^{-1} PA published in [13]. This PA has a peak power added efficiency (PAE) of 78% at 3.5 GHz. A block diagram of the measurement setup used to perform the experiments is shown in Fig. 8. A Tektronix Arbitrary Waveform-Generator (AWG7102), which is running at 10 GSa/s with 10 bit resolution, was used to create the modulated RF-carrier. A low-pass filter with a cutoff-frequency of 6 GHz was connected in between the AWG and the driver in order to filter out any spurious components from the AWG. The waveform uploaded to the AWG was generated in MATLAB using the complex baseband model as presented in Fig. 3. A single carrier, 5 MHz W-CDMA signal with 6.8 dB PAPR was encoded using an optimized $\Sigma\Delta$-modulator [20]. An Agilent Infiniium 54854 real-time oscilloscope (RTO) was used to measure both the input and output signals to and from the PA.

Further on, due to the bandwidth limitation imposed by the power amplifier and the RTO, which has a cutoff frequency of 4 GHz, the bandwidth of the composite signal $|S_{q,c}|$ was limited to 1 GHz (3.5 ± 0.5 GHz) using an ideal low-pass filter in MATLAB. The RTO was operated at a sampling rate of 20 GSa/s, with 8 bit resolution. The input power was adjusted to drive the signal peaks, after clipping, into compression of the amplifier. In all illustrative examples, $f_s = 100$ MHz and $BW_c = f_s/4$ are used.

The measured drain efficiencies, η, were then calculated using the total delivered output power, including the quantization noise power. The efficiency measurements can therefore give insight into the intrinsic efficiency of the PA without having to solve the complex issue of integrating the output reconstruction filter with the PAs [25]. However, due to the highly idealized assumptions made for the class B model in III and the bandpass characteristics of the actual PA, accurate estimations of absolute η figures should not be expected.

B. Simulations

The first experiment investigates the relationship between signal to noise ratio and drain efficiency for various clipping probabilities. A common method to predict η for narrowband signals with a given amplifier, is to use measurement data from a static power sweep in combination with the signal statistics, [26]. Fig. 9 shows such an example where a static power sweep performed on a class F^{-1} GaN amplifier [27] is used, in combination with an SNR calculation based on simulation using a data record of 10^6 samples generated as stated in the prerequisites. The result is compared to the ideal class B based efficiency estimate, η_B from (37), and the SNR estimate, SNR_{est} from (42). As shown in Fig. 9, there is a fairly good agreement between simulations using the class F^{-1} data, and the theoretical predictions. And as expected, the efficiency can be improved by allowing some clipping of the input signal. This shows that the amplifier used in this experiment, behaves similar to an ideal class B behavior in terms of its efficiency, at least at one single frequency of 3.5 GHz.

Fig. 10a shows the PSD for one of the simulations above where the AWGN-model, derived in III-E, predicts the SNR-performance of the clipped signal at $\mathcal{K} = 1\%$. The simulations
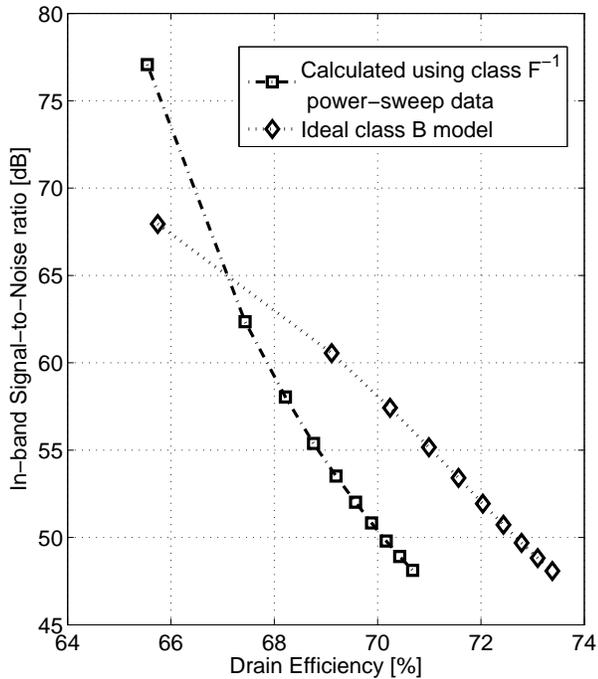
Fig. 9: Drain efficiency (η) and in-band Signal-to-Noise Ratio as a function of clipping probability $\mathcal{K}$ with $BW_c = f_s/4$. Both calculated using record data (squares) and the combination of η_B and SNR_{est} predictions (diamonds), as described in section III-E. Markers denote the simulated clipping probabilities $\mathcal{K}$, starting from 0.5% and ranging to 5%, in steps of 0.5%.

indicate 58.9 dBc, while the AWGN approximation predicts an SNR_{est} of 58.4 dBc. Further on, Fig. 10b illustrates the accuracy of the AWGN-model over values of $\mathcal{K}$ up to 5%. Fig. 9 shows calculated η_B and SNR_{est}, using the models derived in section III, compared to simulated η using the class F^{-1} characteristics and SNR simulated using an actual signal record.

Using the expression stated in (37) combined with the AWGN-model, we can now easily find a suitable value for $\mathcal{K}$ given our spectral mask and SNR requirements, while maximizing η.

C. Measurements

A variety of modulated measurements were made at $f_s = 50, 80$ and 100 MHz, with different compensation bandwidths, ranging between $10 - 50\%$ and using the hardware setup described in the prerequisites. The measured drain efficiency is presented in Fig. 11 as a function of the fractional compensation bandwidth, BW_c/f_s. A very moderate clipping probability of $\mathcal{K} = 0.1\%$ was used in all cases in order to keep SNR below -60 dBc with good margin.

The results from the ideal class B model, as presented in the previous section, is presented in the same figure. The computations of η_B were made using values of σ_c^2 numerically
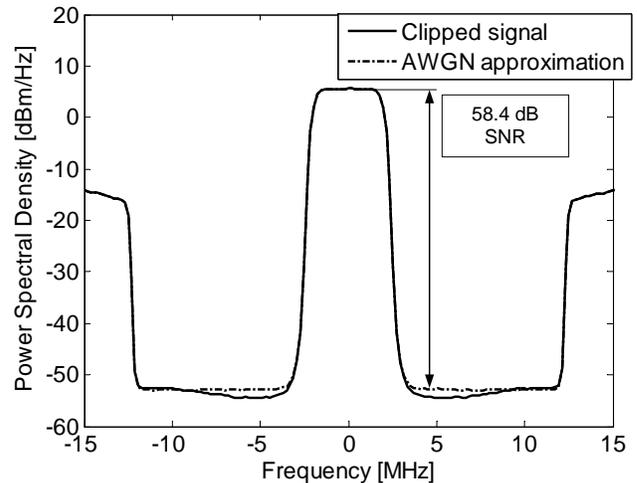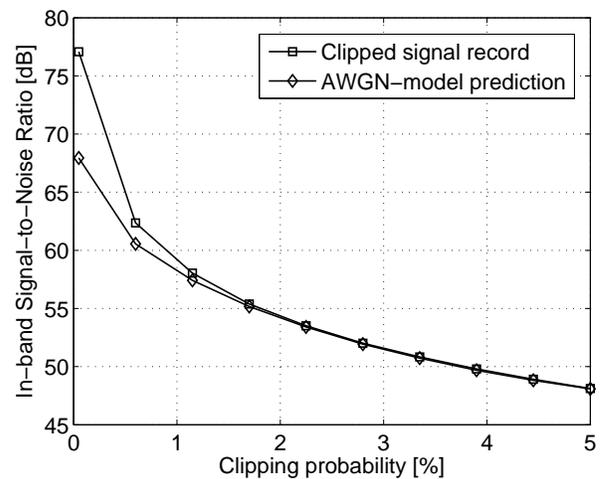
Fig. 10: (a) Simulated PSD with $\mathcal{K} = 1\%$, yielding a calculated SNR of 58.9 dBc and an estimated SNR_{est} of 58.4 dB, within the relevant frequency band BW_c. (b) SNR-calculations from both a clipped signal record and the SNR_{est} calculated using the AWGN-approximation for values of clipping probabilities $\mathcal{K}$ ranging from 0.05% to 5% (from left to right).

estimated from the signal record. It should be noticed that although the model shows a similar trend of η as a function of the relative compensation bandwidth, BW_c/f_s, quite large deviations can be spotted. The results does however confirm the relation between the fractional compensation bandwidth, clipping probability and drain efficiency.

Since the idealized class B model assumes infinite bandwidth, i.e. that the input-output relation is constant for all frequencies and amplitudes, and no gain compression, comparison of absolute efficiency figures between the highly idealized class B model and the measured results are generally not valid. Thus, for the cases of extremely wideband signals with peaks entering the compression region of the amplifier, as presented here, a large prediction error should be expected, unless the prediction model is further developed in order to incorporate
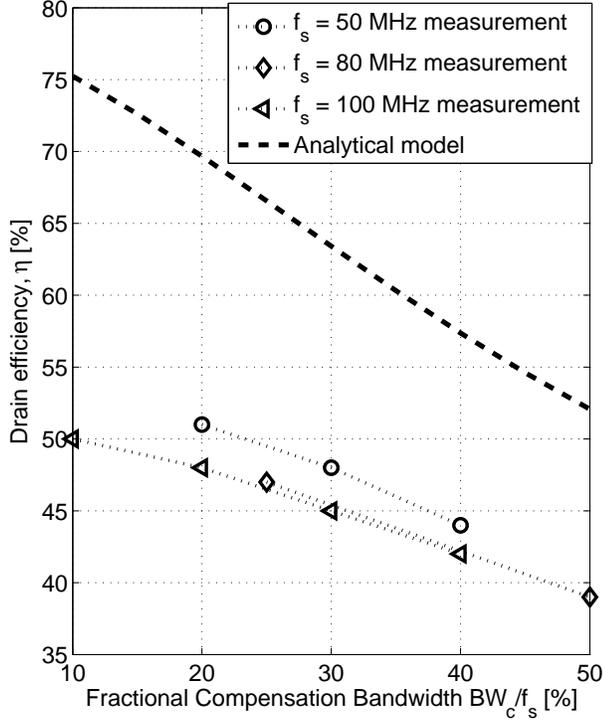
Fig. 11: A summary of measured η and calculated η_B, both as a function of the fractional compensation bandwidth, BW_c/f_s. For the analytical model, η_B, σ_c^2 has been calculated as described in section III-C, as a function of BW_c/f_s.

these effects, [28]. The ideal class B model should therefore merely be considered as an analysis tool for identification of efficiency trends as a function of $\mathcal{K}$ and BW_c/f_s.

One example of the measured input and output spectrum is presented in both Fig. 12a and Fig. 12b, where $f_s = 100$ MHz and $BW_c = 40$ MHz. The measured SNR of the input signal is however limited due to the 8-bit resolution of the RTO to $\text{SNR}_{\min} = 1.76 + 6.02 \cdot 8 \approx 50$ dB. An SNR of approximately 34.4 dBc is measured at the PA output in this case, which points toward the need for a pre-distorter [12].

V. GENERALIZATION OF PROPOSED ARCHITECTURE

The methodology developed and analyzed in section II-III can be generalized and used in combination with a wide range of pulsed RF transmitter architectures. For the purpose of illustration, modifications of the developed theory for two cases of pulsed transmitters are discussed here.

A. Multi-level carrier bursting transmitters

For multi-stage power amplifier topologies with several high efficiency areas, such as for example the Doherty amplifier [7], [29], a topology using a $\Sigma\Delta$-modulator with a M-step quantizer can be used. Such $M + 1$-level topology generates a signal $|S'_{q,c}[n]|$, which envelope PDF is a Rician mixture of
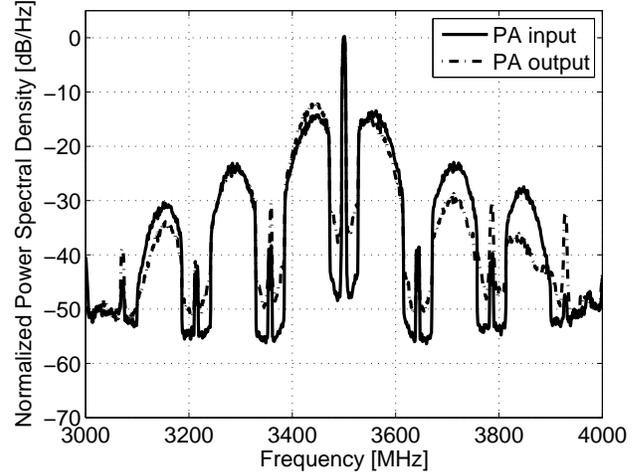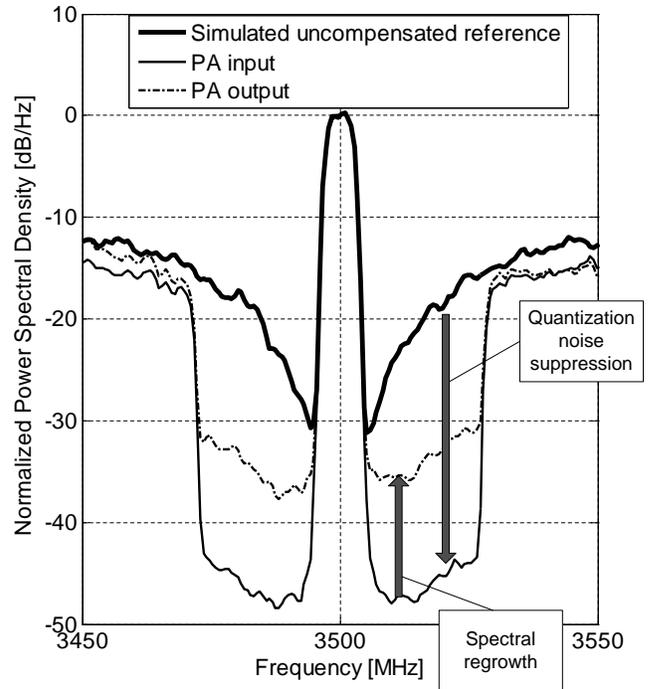
Fig. 12: (a) Measured PSD of the signal using $f_s = 100$ MHz, with $BW_c = 40$ MHz and a pre-filtering of 1 GHz. (b) Closeup of the PSD around $f_c = 3.5$ GHz and the compensation band, BW_c.

$M + 1$ components, described in the same manner as (25) with

$$p_{|S'_{q,c}|}(s|\boldsymbol{\nu},\boldsymbol{\sigma}) = \sum_{i=0}^{M} \lambda_i \mathbf{I}_{[0,1]}(s) r_{|S_{q,c}|}(s|K\nu_i, \sigma_{kc}) + \mathcal{K}\delta(s-1) \tag{43}$$

where

$$\boldsymbol{\nu} = \{\nu_0, \nu_1, \ldots, \nu_{M-2}, \nu_M\} \tag{44}$$

are the M quantizer states of the $\Sigma\Delta$-modulator and

$$\boldsymbol{\sigma} = \underbrace{\{\sigma_{kc}, \dots, \sigma_{kc}\}}_{M+1 \text{ times}}, \qquad (45)$$

where $\sigma_{kc}^2 = K^2\sigma_c^2$ is the normalized variance of the compensation signal $c[n]$. The normalization constant K is calculated by modifying (23) as

$$K = \frac{1}{1 + \sqrt{2}\sigma_c \text{erfc}^{-1}\left[\frac{2\mathcal{K}}{\lambda_M}\right]}. \qquad (46)$$

One advantage of such multi-level architecture over the binary case is that following classical $\Sigma\Delta$-modulation theory [22] and the results given in (28), σ_c^2 for a given BW_c is reduced by increasing M due to the reduction of the total quantization noise power σ_q^2. Assuming that 1 represents the maximum output power and that the M-step quantizer is uniform with $\Delta = 1/M$, we can rescale σ_q^2 in (29) as

$$\sigma_q^2 = \frac{1}{12M^2} < \frac{1}{12} \qquad (47)$$

for all integer $M > 1$.

B. Cartesian architectures

Cartesian pulsed RF transmitter architectures, as described in [30], [28], are constructed by applying binary $\Sigma\Delta$-modulation to I and Q separately before recombining and up-converting to RF. The method for applying bandpass quantization noise cancellation has been previously described in [31, Fig. 3.11, p. 23, eq. (3.14)], but without any detailed analysis of the signal PDF.

Due to the constant envelope of the quantized signal, $A_q[n] = 1$, which comes from the use of a symmetric $\pm 1/\sqrt{2}$ quantizer on the orthogonal quadrature components, the resulting signal PDF of $|S'_{q,c}[n]|$ is a simple unimodal Rice distribution,

$$p_{|S'_{q,c}|}(s|K, \sigma_{kc}) = \mathbf{I}_{[0,1]}(s)r_{|S_{q,c}|}(s|K, \sigma_{kc}) + \mathcal{K}\delta(s-1) \quad (48)$$

where the normalization factor K is calculated as

$$K = \frac{1}{\sqrt{2}\left(1 + \sigma_c \text{erfc}^{-1}[2\mathcal{K}]\right)}. \qquad (49)$$

In this scenario, the quantization noise cancellation capability is limited for high PAPR signals due to the quantization points placement around the unit circle. Thus, as PAPR increases, σ_c^2 will grow more rapidly than in the carrier bursting case, since this includes a "off"-state.

From (29) it also stands clear that the quantization noise power, σ_q^2, is increased, since $\Delta = \sqrt{2}$, which gives

$$\sigma_q^2 = \frac{2}{12} = \frac{1}{6} > \frac{1}{12M^2} \qquad (50)$$

for all integer $M \geq 1$.

C. Simulations

In order to illustrate the generalizations of the proposed concept described in the two previous sections, modifications of the equivalent complex baseband model described in section II were done. Fig. 13 shows the resulting PDFs for both the Cartesian $\Sigma\Delta$ and the 2- and 3-level carrier bursting transmitters.
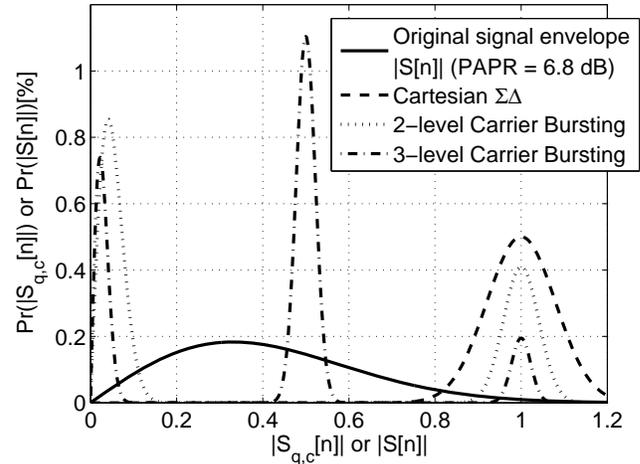
Fig. 13: Simulated PDFs of $|S[n]|$ and $|S_{q,c}[n]|$ for Cartesian $\Sigma\Delta$-modulation, 2- and 3-level carrier bursting given $BW_c = f_s/4$.

VI. Conclusions

A method for suppressing the passband quantization distortion in pulsed transmitter architectures has been suggested. The method enables the use of more wideband RF filters for signal reconstruction, with less insertion loss which decreases the power dissipated within the filter. The suppression is performed by superimposing a controlled amplitude component on to the pulses.

An equivalent complex baseband model has been analyzed and mathematical expressions governing the suppression mechanism has been derived and studied. The impact on the power efficiency of the system parameters, the cancellation signal variance and the clipping probability, has been studied by means of a theoretical model based on the ideal class B amplifier. The first being mainly determined by the NSC settings of the $\Sigma\Delta$-modulator and the ratio of compensation bandwidth to pulse-rate, BW_c/f_s, as shown. The second parameter is set by the hard limiter using an AWGN-based SNR-prediction model. Using the analysis the optimum trade-off between these parameters can be obtained. This provides a certain flexibility which makes the system suitable for multi-standard communication systems.

Numerical computations were performed using a 1 carrier W-CDMA signal with 6.8 dB PAPR. Measurements on a high efficiency inverse class F PA working at 3.5 GHz shows good potential for high efficiency, high bandwidth operation without the need of exceedingly high pulse rates, while still providing a good noise free dynamic range over a fairly large bandwidth. In turn, this relaxes the demands on the relative bandwidth of the reconstruction filter with decreased filter losses and improved efficiency as a result. Finally, generalizations of the proposed architecture toward a larger class of pulsed RF transmitters is discussed by means of two different examples.

REFERENCES

[1] W. Doherty, "A new high efficiency power amplifier for modulated waves," *Proceedings of the IRE*, vol. 24, no. 9, pp. 1163–1182, Sept. 1936.

[2] H. Chireix, "High power outphasing modulation," *Proceedings of the IRE*, vol. 23, no. 11, pp. 1370–1392, Nov. 1935.

[3] L. Kahn, "Single-sideband transmission by envelope elimination and restoration," *Proceedings of the IRE*, vol. 40, no. 7, pp. 803–806, July 1952.

[4] N. Jayant and P. Noll, *Digital coding of waveforms*. Prentice Hall, Signal Processing Series, ISBN 0-13-211913-7, 1984.

[5] F. Raab, "Radio frequency pulsewidth modulation," *IEEE Trans. Commun.*, vol. 21, no. 8, pp. 958– 966, Aug. 1973.

[6] F. H. Raab, P. Asbeck, S. Cripps, P. B. Kenington, Z. B. Popovic, N. Pothecary, J. F. Sevic, and N. O. Sokal, "RF and microwave power amplifier and transmitter technologies - part 5," *High Frequency Electronics*, vol. 3, no. 1, pp. 46 – 54, Jan. 2004.

[7] L. Shu-Hsien and Y. Wang, "High efficiency WCDMA power amplifier with pulsed load modulation (PLM)," *IEEE J. Solid-State Circuits*, vol. 45, no. 10, pp. 2030 –2037, Oct. 2010.

[8] T. Matsuura and H. Adachi, "A high efficiency transmitter with a Delta-Sigma modulator and a noise cancellation circuit," in *European conference on wireless technology*, 2004.

[9] W. Ahmed, "Quantization noise suppression in digitally segmented amplifiers," *IEEE Trans. Circuits Syst. I*, vol. 56, no. 3, pp. 529–540, March 2009.

[10] R. Schreier, "Noise-shaped coding," Ph.D. dissertation, University of Toronto, Toronto, Canada, May 1991. [Online]. Available: http://www.dissonance.com/archive/phd/schreier.pdf

[11] J. C. Candy and G. C. Temes, Eds., *Oversampling Delta-Sigma Data Converters Theory, Design and Simulation*. New York: IEEE Press., 1992.

[12] U. Gustavsson, T. Eriksson, and C. Fager, "A General Method for Quantization Noise Suppression in Pulsed Transmitter Architectures," in *Proc. IEEE International Microwave Symposium*, Boston, USA, June 2009, p. 1529 1532.

[13] P. Saad, C. Fager, H. Nemati, H. Cao, H. Zirath, and K. Andersson, "A highly efficient 3.5 Ghz inverse class-F GaN HEMT power amplifier," in *International Journal of Microwave and Wireless Technologies*, 2010, pp. 317–324.

[14] S. Norsworthy, R. Schreier, and G. Temes, *Delta-Sigma Data Converters (Theory, Design, and Simulation)*, 1st ed. Wiley-IEEE Press, 1996.

[15] A. Grebennikov, *RF and Microwave Power Amplifier Design*, 1st ed. McGraw-Hill, 2005.

[16] S. Haykin, *Digital Communications*, 1st ed. John Wiley and sons, 1988.

[17] S. Rice, "Mathematical analysis of random noise," *Bell System Technical Journal*, 1945.

[18] G. Grimmett and D. Stirzaker, *Probability and Random Processes*, 3rd ed. Oxford University Press, 2001.

[19] D. M. Pozar, *Microwave and RF Design of Wireless Systems*, 1st ed. John Wiley and Sons, 2000.

[20] U. Gustavsson, T. Eriksson, and C. Fager, "Quantization noise minimization in $\Sigma\Delta$-modulation based RF transmitter architectures," *IEEE Trans. Circuits Syst. I*, vol. 57, no. 12, pp. 3082 –3091, Dec. 2010.

[21] J. G. Proakis and D. G. Manolakis, *Digital Signal Processing - Principles, Algorithms and Applications*, 4th ed. Prentice Hall, 2007.

[22] R. Schreier and G. Temes, *Understanding Delta-Sigma Data Converters*. New Jersey: Wiley Interscience, 2005.

[23] J. G. Proakis and M. Salehi, *Digital Communications*, 5th ed. McGraw-Hill, 2008.

[24] W. H. Greene, *Econometric analysis*, 5th ed. Prentice Hall, 2002.

[25] C. Schuberth, P. Singerl, M. Gadringer, H. Arthaber, A. Wiesbauer, and G. Magerl, "Highly efficient switched-mode transmitter using a current mode class-D RF amplifier," *International Journal of RF and Microwave Computer-Aided Engineering*, vol. 20, no. 4, pp. 446–457, 2010.

[26] H. M. Nemati, C. Fager, M. Thorsell, and H. Zirath, "Characterization of switched mode LDMOS and GaN power amplifiers for optimal use in polar transmitter architectures," *Microwave Symposium Digest, 2008 IEEE MTT-S International*, 2008.

[27] P. Saad, H. Nemati, M. Thorsell, K. Andersson, and C. Fager, "An Inverse Class-F GaN HEMT Power Amplifier with 78% PAE at 3.5 GHz," in *Microwave Conference, 2009. EuMC 2009. European*, sept. 2009, pp. 496 –499.

[28] F. Ghannouchi, S. Hatami, P. Aflaki, M. Helaoui, and R. Negra, "Accurate power efficiency estimation of GHz wireless delta-sigma transmitters for different classes of switching mode power amplifiers," *IEEE Trans. Microwave Theory Tech.*, vol. 58, no. 11, pp. 2812 –2819, Nov. 2010.

[29] M. Pelk, W. Neo, J. Gajadharsing, R. Pengelly, and L. de Vreede, "A high-efficiency 100-w gan three-way doherty amplifier for base-station applications," *IEEE Trans. Microwave Theory Tech.*, vol. 56, no. 7, pp. 1582 –1591, July 2008.

[30] P. Kenington, *RF and Baseband Techniques for Software Defined Radio*. Boston: Artech House Publishers, 2005.

[31] U. Gustavsson, "Quantization and Noise-Shaped Coding for High Efficiency Transmitter Architectures," *Licentiate Thesis, Chalmers University of Technology*, vol. ISSN 1652-0769, May 2009, http://publications.lib.chalmers.se/cpl/record/index.xsql?pubid=92634.